Magnetic structures of the anisotropic intermetallic compounds Er_2CoGa_8 and Tm_2CoGa_8

R. D. Johnson,[1,*] T. Frawley,[1] P. Manuel,[2] D. D. Khalyavin,[2] C. Adriano,[3] C. Giles,[3] P. G. Pagliuso,[3] and P. D. Hatton[1]
[1]*Department of Physics, Durham University, South Road, Durham DH1 3LE, United Kingdom*
[2]*ISIS Facility, Rutherford Appleton Laboratory, STFC, Chilton, Didcot, Oxon OX11 0QX, United Kingdom*
[3]*Instituto de Física Gleb Wataghin, Universidade Estadual de Campinas, 13083-970 Campinas, SP, Brazil*
(Received 29 March 2010; revised manuscript received 30 June 2010; published 8 September 2010)

Two members of the isostructural R_2CoGa_8 intermetallic series, Er_2CoGa_8 and Tm_2CoGa_8, have been studied by powder neutron diffraction. Antiferromagnetic ordering of the rare-earth sublattices was confirmed to occur at 3.0 K and 2.0 K, respectively. Furthermore, determination of the critical exponent showed Er_2CoGa_8 to adopt a three-dimensional universality class. In spite of a common magnetic easy axis and similar structural characteristics, the antiferromagnetic structures were found to be different for the erbium- and thulium-based compounds. The corresponding magnetic space groups were determined to be $P_{2a}mmm'$ and P_Cmmm. The difference in magnetic structures is discussed based on crystal electric field effects that are known to be prevalent in such materials.

DOI: 10.1103/PhysRevB.82.104407 PACS number(s): 71.20.Eh, 75.25.−j, 61.05.F−, 75.10.Dg

I. INTRODUCTION

Rare-earth intermetallic compounds are a class of material that exhibit a diverse range of fascinating physical properties. For example heavy-fermion behavior, Kondo ground states, quantum criticality, and pressure-induced superconductivity have all been found.[1–5] These phenomena are likely to be due to the competition of microscopic electronic interactions such as the magnetism and crystal electric field (CEF).[6–8] A common theme in many intermetallics is the dependence of the electronic properties on the rare-earth ion. For example, $CeCu_2Si_2$ was found to undergo a transition into a superconducting state below ~1 K that did not comply with the conventional Bardeen-Cooper-Schrieffer theory of superconductivity. However, $LaCu_2Si_2$ remains in a normal state down to 50 mK.[9] Further, a number of different magnetic structures have been measured across the series, solely dependent upon the choice of rare-earth ion.[10] The role of the rare-earth ion in the microscopic behavior of these systems remains an important question, specifically the interaction of the 4*f* magnetism with the CEF. In this paper we concentrate on the newly synthesized R_2CoGa_8 series, which has been shown to exhibit a strong coupling between the 4*f* magnetism and the CEF.[11] Consequently, a variety of electronic properties have been shown to be dependent upon the rare-earth ion.[11,12]

The R_2CoGa_8 series is limited to R=Gd-Lu and Y due to an instability in the crystallization of the lighter rare-earth compounds.[11–13] The series is isostructural, adopting at room temperature the tetragonal space group $P4/mmm$. This type of structure hosts a number of recently discovered heavy-fermion superconductors such as Ce_2CoIn_8,[1] Ce_2RhIn_8,[2] and Ce_2PdIn_8.[14] The crystal structure can be thought of as a stacking of RGa_3 units between $CoGa_2$ layers in the direction of the fourfold tetragonal axis. A thorough survey of magnetization and transport properties was published by Joshi *et al.*,[11,12] in which an in-depth comparison between the R_2CoGa_8 series and other rare-earth intermetallic compounds was presented. Of particular interest is the dependence of the magnetic anisotropy upon the rare-earth ion radii. This splits the series into four groups. These are the diamagnetic compounds with R=Y and Lu, isotropic Gd_2CoGa_8 (as for Gd^{3+} L=0), R=Tb, Dy, and Ho compounds with a magnetization easy axis parallel to the *c* axis and finally R=Er and Tm compounds, which have a magnetization easy axis perpendicular to the *c* axis. In this study we focus on the latter erbium and thulium based members. The two compounds antiferromagnetically order at T_N=3.0 K and 2.0 K, respectively,[11] and Er_2CoGa_8 is on the border between having a magnetization easy axis parallel or perpendicular to the *c* axis.

In order to properly explain the bulk magnetic properties one must account for CEF effects. This is particularly apparent through CEF calculations that can explain the rare-earth-dependent anisotropy of magnetization,[11] correctly predicting the direction of the magnetic easy axis and its dependence on rare-earth substitution. Furthermore, across the series, the antiferromagnetic transition temperatures are found to be higher than those predicted by de Gennes scaling. This can also be explained through CEF calculations.[11]

To better understand the varied macroscopic properties of intermetallic materials we require a probe of the microscopic electronic ordering phenomena. The only previously published magnetic structure of any member of the R_2CoGa_8 series was that of Ho_2CoGa_8, determined by resonant magnetic x-ray scattering.[15] We have performed the first neutron diffraction study of this intermetallic series. We show that Er_2CoGa_8 and Tm_2CoGa_8 develop collinear antiferromagnetic structures below their respective Néel temperatures. In both materials, magnetic moments align parallel to the *b* axis, however they differ in propagation vector, $\mathbf{k}=(0,1/2,0)$ for Er_2CoGa_8 and $\mathbf{k}=(1/2,0,1/2)$ for Tm_2CoGa_8, due to CEF effects.

II. EXPERIMENT

Single-crystal samples of Er_2CoGa_8 and Tm_2CoGa_8 were grown by the gallium flux technique.[16] Laboratory-based x-ray powder diffraction confirmed the Er_2CoGa_8 and Tm_2CoGa_8 room-temperature crystal structures to be tetrag-

TABLE I. Lattice parameters refined from neutron powder data of Er_2CoGa_8 and Tm_2CoGa_8, measured at 300 mK.

Sample	Space group	a (Å)	c (Å)
Er_2CoGa_8	$P4/mmm$	4.20195(5)	10.9438(2)
Tm_2CoGa_8	$P4/mmm$	4.18980(7)	10.9109(3)

onal ($P4/mmm$) with lattice parameters $a=4.210(5)$ Å and $c=10.96(1)$ Å, and $a=4.202(5)$ Å and $c=10.95(1)$ Å, respectively. Approximately 1 g of each sample was prepared for neutron powder diffraction by grinding selected single crystals using an agate pestle and mortar, resulting in fine powders of consistent grain size.

Neutron powder diffraction data were collected on both samples using the WISH time of flight instrument on the second target station at the ISIS facility.[17] A ^{3}He sorption insert was employed within a standard Oxford Instruments cryostat to achieve sample temperatures of less than 300 mK. Each sample was loaded into a 6 mm diameter vanadium can with a thick copper head, covered with a Cd mask, placed in contact with the ^{3}He pot. A copper wire (cold finger) was run through the length of the can to ensure better thermal conductivity through the sample. Data were collected with high counting statistics above T_N and at 300 mK, the base temperature of the ^{3}He insert. Shorter data collections were performed upon warming through the transition to determine the temperature dependence of the magnetic scattered intensity. Determinations of the nuclear and magnetic structures were performed using the FULLPROF suite of programs.[18]

III. RESULTS AND DISCUSSION

The crystal structures of both compounds were refined above, and below, the respective magnetic transitions in the tetragonal $P4/mmm$ space group, as has been reported for Ho_2CoGa_8.[11] In order to properly reproduce the experimental data, it was necessary to account for additional reflections due to extraneous scatter from the sample can. We therefore included in the refinements a copper nuclear phase (Cu cold finger). This phase was fitted by Le Bail intensity fitting as the copper wire was found to be extremely textured. In both samples we found no detectable changes of structural parameters above and below the magnetic transition, indicating that magnetoelastic coupling was negligibly small. We therefore only present the refinements of data measured below T_N at 300 mK. The lattice parameters and fractional coordinates of the inequivalent atom sites are presented in Tables I and II.

Figures 1 and 2 show the 300 mK neutron diffraction pattern and Rietveld refinements of both samples. By comparison between the powder patterns measured above T_N (not shown here) and at 300 mK, a large number of additional magnetic reflections became evident. We investigated the behavior of the magnetic phase upon warming through the transition. The integrated intensities of selected magnetic diffraction peaks are plotted as a function of temperature in Fig. 3, clearly showing transition temperatures of 3.0 K and 2.0 K

TABLE II. Structural and magnetic parameters of Er_2CoGa_8 and Tm_2CoGa_8, refined from data collected at 300 mK. The direction of the magnetic moments of the rare-earth ions are chosen to lie parallel to the b axis (as opposed to the a axis).

Atom	x	y	z	Moment ($\mu_B \parallel b$)
		Er_2CoGa_8, $\mathbf{k}=(0,1/2,0)$		
Er (1)	0	0	0.3068(3)	4.71(3)
Er (2)	0	0	−0.3068(3)	−4.71(3)
Co	0	0	0	
Ga (1)	0	0.5	0.5	
Ga (2)	0.5	0.5	0.2952(5)	
Ga (3)	0	0.5	0.1177(2)	
		Tm_2CoGa_8, $\mathbf{k}=(1/2,0,1/2)$		
Tm (1)	0	0	0.2964(7)	2.35(4)
Tm (2)	0	0	−0.2964(7)	−2.35(4)
Co	0	0	0	
Ga (1)	0	0.5	0.5	
Ga (2)	0.5	0.5	0.3100(6)	
Ga (3)	0	0.5	0.1176(2)	

for Er_2CoGa_8 and Tm_2CoGa_8, respectively. This is in agreement with bulk magnetometry results.[11] Further, by fitting a power law to the Er_2CoGa_8 data (the Tm_2CoGa_8 data is insufficient for fitting) we find a critical exponent of $\beta=0.33\pm0.02$, suggesting that these compounds adopt either the 3D-Ising or 3D-XY universality class.[19] In either case we predict a three-dimensional magnetic system with one-dimensional or two-dimensional order parameters, respectively.

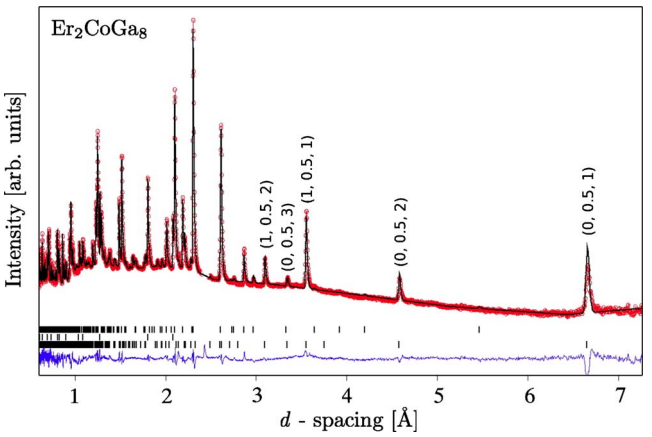

FIG. 1. (Color online) Rietveld refinement pattern for Er_2CoGa_8 at 300 mK. Only data from bank 3 (average $2\theta=90°$) of the WISH instrument was required to achieve high resolution over a sufficiently large time of flight interval to capture all the magnetic reflections. The top, middle, and bottom tick marks refer to Er_2CoGa_8-nuclear, Cu-nuclear (cold finger), and Er_2CoGa_8-magnetic phases, respectively. The difference pattern is shown at the bottom of the figure. A number of prominent magnetic reflections are indexed.

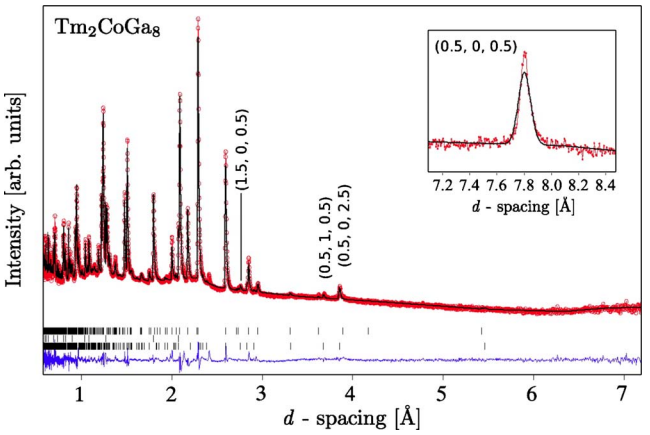

FIG. 2. (Color online) Rietveld refinement pattern for Tm_2CoGa_8 at 300 mK. Data from bank 3 (average $2\theta=90°$) of the WISH instrument is shown in the main pane, however it was necessary to incorporate data from bank 2 (average $2\theta=58.33°$) into the refinement in order to capture all high d-spacing magnetic reflections (shown in inset). The top, middle, and bottom tick marks refer to Tm_2CoGa_8-nuclear, Cu-nuclear (cold finger), and Tm_2CoGa_8-magnetic phases, respectively. The difference pattern is shown at the bottom of the figure. A number of prominent magnetic reflections are indexed.

In the refinement of the magnetic structures, it was assumed that only the rare-earth ions are magnetic. The cobalt ions are expected to be nonmagnetic due to an effective filling of the transition metal $3d$ states by an excess of gallium $4p$ electrons in the conduction band.[20] This is confirmed by the fact that Y_2CoGa_8 and Lu_2CoGa_8 are diamagnetic metals. Furthermore, the low transition temperatures are a signature of probable rare-earth ordering.

Despite having very similar crystal structures and common magnetic easy axes,[11] the 300 mK diffraction patterns (Fig. 1 and 2) clearly show that the two samples have different magnetic propagation vectors. These were determined to

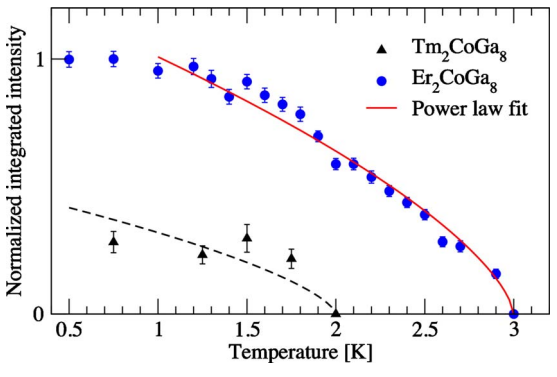

FIG. 3. (Color online) The temperature dependence of the integrated intensity of a selected magnetic reflection of both Er_2CoGa_8 ($d\simeq 3.56$ Å) and Tm_2CoGa_8 ($d\simeq 3.86$ Å), shown as blue circles and black triangles, respectively. A power law has been fitted to the Er_2CoGa_8 data (solid red line), giving a critical exponent of $\beta=0.33\pm0.02$ and $T_N=3.00\pm0.01$ K. The Tm_2CoGa_8 data was not of sufficient quality to obtain a reliable fit, however the transition at $T_N=2$ K is clear. A scaled power law with the same exponent as that fitted to the Er_2CoGa_8 data is overlaid (broken black line).

TABLE III. Reliability factors of refinements of the six possible single-irrep magnetic structure models for both Er_2CoGa_8 and Tm_2CoGa_8.

Moment axis	c axis stacking	R_{Mag}	R_{Bragg}	χ^2
	Er_2CoGa_8, $\mathbf{k}=(0,1/2,0)$			
a	(++++)	67.5	11.7	43.4
a	(+−+−)	68.7	9.1	29.3
b	(++++)	75.7	11.0	42.4
b	(+−+−)	**14.7**	**7.3**	**8.9**
c	(++++)	83.6	11.7	44.3
c	(+−+−)	45.5	9.7	20.0
	Tm_2CoGa_8, $\mathbf{k}=(1/2,0,1/2)$			
a	(+−−+)	102.0	9.0	14.3
a	(++−−)	54.4	7.5	12.1
b	(+−−+)	114.3	9.1	14.4
b	(++−−)	**21.4**	**6.9**	**10.3**
c	(+−−+)	93.9	9.0	14.4
c	(++−−)	50.8	7.7	12.5

be associated with the X[$\mathbf{k}=(0,1/2,0)$] and R[$\mathbf{k}=(1/2,0,1/2)$] points of symmetry (Miller and Love notations[21]) for the erbium and thulium compositions, respectively. In tetragonal symmetry, the choice of the a and b axes is arbitrary when defining the propagation vectors. The important consideration is the direction of the magnetic moments in the ab plane with respect to the propagation vector. Here, the a and b axes have been defined such that the magnetic moments lie parallel to the b axis, as will become apparent later. In both cases there are eight one-dimensional irreducible representations (irreps) associated with the corresponding wave vector groups. Six of them enter into the global reducible magnetic representation on the $2g$ Wyckoff position of the $P4/mmm$ space group occupied by Er or Tm. The symmetrized combinations of the axial vectors transforming as basis functions of these irreps correspond to the moment directions along the a, b, and c axes with parallel and antiparallel alignment on the Er/Tm(1) and Er/Tm(2) sites.

Magnetic structure refinements corresponding to the six possible single-irrep models were performed for each sample. The magnetic and structural reliability factors (R_{Mag} and R_{Bragg}) and χ^2 for the refinements are given in Table III. It is clear that for each sample only a single model successfully fits the data, as highlighted in bold in Table III and shown in Figs. 1 and 2. We note that for all Tm_2CoGa_8 models, the χ^2 values are similar. This is due to the magnetic reflections being weak compared to both the structural reflections and the background. However the R_{Mag} values, which are also large due to the weak magnetic reflections, clearly show the correct model. For both Er_2CoGa_8 and Tm_2CoGa_8, the fitted magnetic structures correspond to moment directions aligned parallel to the b axis (with respect to our defined propagation vectors) and an AFM stacking along the c axis of (+−+−) and (++−−), respectively. In a magnetic reso-

nant x-ray diffraction study on Ho_2CoGa_8 (Ref. 15) it was not possible to determine whether the holmium moments stacked (++−−) or (+−−+) along the *c* axis. Tm_2CoGa_8 also adopts a similar *c* axis stacking, however our results are not ambiguous, and clearly show a single magnetic structure solution.

It should be pointed out that the wave vector stars related to the X and R reciprocal points both consists of two arms. The corresponding noncollinear two-**k** magnetic structures are undistinguishable from the discussed above collinear single-**k** models in the powder diffraction experiments. The discrimination can be done only based on monodomain single-crystal measurements or based on observation of nuclear satellite reflections associated with the M[**k** $=(1/2,1/2,0)$] reciprocal point and having a specific critical behavior. These reflections are expected in the case of the two-**k** structures due to the presence of appropriate coupling invariants in a polynomial decomposition of the Landau free energy. The observation of these extremely weak reflections is a difficult experimental task and is possible only in single crystal measurements. However, taking into account the simple exchange topology of the rare-earth sublattice in R_2CoGa_8, without geometrical frustration, the noncollinear two-**k** structures are considered here to be unlikely.

The magnitudes of the magnetic moments at 300 mK were refined to be $4.71(3)\mu_B$/Er and $2.35(4)\mu_B$/Tm, as given in Table II. These values are in good agreement with those obtained from bulk magnetization measurements; extrapolating the isothermal magnetization data measured by Joshi *et al.*[11] gives zero field magnetic moments of $4.6\pm0.1\mu_B$/Er and $2.90\pm0.03\mu_B$/Tm. The rare-earth ion moments are found to be much smaller than their theoretical free-ion values of $9\mu_B$/Er and $7\mu_B$/Tm. This is expected in such systems where the magnetic behavior is dominated by CEF effects.[10]

The ground state multiplet degeneracy of the R^{3+} ions is lifted by the CEF. The wave functions of the split energy levels were calculated from the CEF parameters found by Joshi *et al.*,[11] in terms of the basis states $|J,J_z\rangle$, using the MCPHASE software package.[22] The zero-field ground states of both Er^{3+} (doublet) and Tm^{3+} (singlet) are nonmagnetic. The state energies and associated $\langle J_z\rangle$ were calculated as a function of internal magnetic field. For Er^{3+}, $\langle J_z\rangle=4.0\mu_B$ in the field range 18–47 T, and for Tm^{3+}, $\langle J_z\rangle=2.7\mu_B$ in the field range 1.5–76 T. These values, clearly illustrating the reduction in moment due to the CEF, are close to those determined from neutron powder diffraction. The deviation from the empirically determined values is likely to be due to uncertainties in the CEF parameters, upon which the calculation is based.

In Er_2CoGa_8 magnetism propagates antiferromagnetically (AFM) along the *b* axis in the direction of the moments, which ferromagnetically (FM) couple along the *a* axis (Fig. 4 top). The *ab* planes of rare-earth ions, containing the easy axis of magnetization, are stacked AFM (+−+−) along the *c* axis. The magnetic space group is $P_{2a}mmm'$ (No. 355) (Ref. 23) with lattice vectors being (0,2,0), (0,0,1), and (1,0,0) with respect to the basis of the parent $P4/mmm1'$ gray group. By contrast, in Tm_2CoGa_8 the moments in the *ab* plane align in an opposite fashion to Er_2CoGa_8, i.e., FM

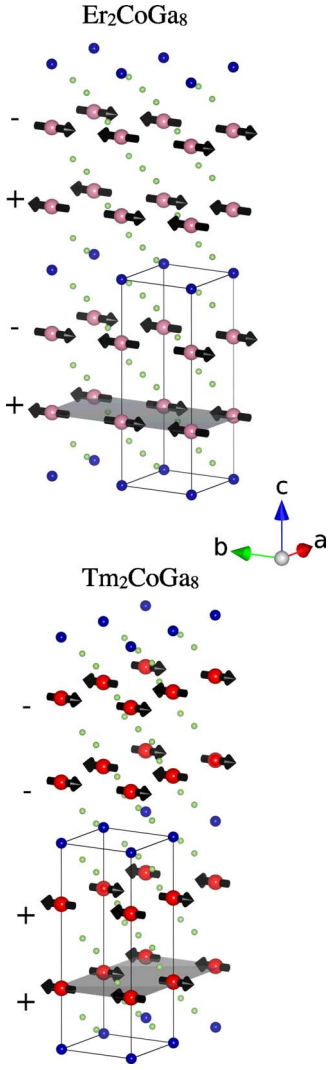

FIG. 4. (Color online) The crystal structure of Er_2CoGa_8 (top) and Tm_2CoGa_8 (bottom) with the respective magnetic structures superimposed, represented by black arrows. Erbium, thulium, cobalt, and gallium ions are shown by pink, red, blue, and green spheres of decreasing size, respectively. The $P4/mmm$ unit cell is drawn in black, and *ab* planes of rare-earth ions are shaded gray.

along the *b* axis and AFM along the *a* axis (Fig. 4 bottom). Furthermore, the planes are stacked alternately FM/AFM along the *c* axis (++−−). This magnetic structure can be described by the P_Cmmm (No. 353) (Ref. 23) space group with (2,0,0), (0,0,−2), and (0,1,0) basis vectors with respect to $P4/mmm1'$.

The above magnetic space groups are orthorhombic and as such the tetragonal symmetry of the crystal structure in the paramagnetic phase must be broken below T_N. There was no evidence in our powder-diffraction data of a lowering of crystal symmetry, however the crystallographic distortions due to the magnetostriction are expected to be extremely small (of the order 10^{-4}–10^{-6}); beyond the instrument resolution. The crystal structure was therefore refined in tetragonal symmetry below T_N, as given above, despite the symmetry lowering. In this scenario the magnetic structure with **k** $=(0,1/2,0)$ and moments parallel to the *b* axis (in the case

of Er_2CoGa_8) is exactly equivalent to a structure with $\mathbf{k}=(1/2,0,0)$ and moments parallel to the *a* axis. In fact, these cases correspond to two different domains associated with the different arms of the same wave vector star. Indeed, refinements of both magnetic structures gave equivalent R_{Mag}, R_{Bragg}, and χ^2.

The spacing of the rare-earth ions is approximately ten times greater than the typical radius of the localized, magnetically ordered rare-earth $4f$ states ($\sim$0.5 Å). There is insufficient overlap of wave functions for direct exchange to occur. The dominant exchange interaction in these compounds is therefore the Ruderman-Kittel-Kasuya-Yosida (RKKY) interaction that supports both FM and AFM exchange, dependent upon the interatomic distances. In competition with the RKKY exchange integral are the CEF terms of the Hamiltonian.[10] As a consequence, rare-earth intermetallic systems may exhibit a wide variety of magnetic structures ranging from collinear FM (Ref. 24) to spin glasses.[25] As both Er_2CoGa_8 and Tm_2CoGa_8 have similar interatomic distances between the rare-earth ions, we suggest that the difference in magnetic structures is due primarily to the CEF terms. Joshi *et al.*[11] showed that the extreme magnetic anisotropy exhibited by this intermetallic series can be accounted for by CEF effects. The magnetic structures refined for Er_2CoGa_8 and Tm_2CoGa_8 clearly give easy axes lying in the *ab* plane. The CEF results in a higher susceptibility in the *ab* plane and the magnetic structure allows for a canting of moments in the same direction. Furthermore, in their calculations of the CEF, they find the in-plane and *c*-axis nearest-neighbor exchange constants to be $\mathcal{J}_{ex}^{ab}/k_B=-0.35$ K and $\mathcal{J}_{ex}^{c}/k_B=-0.32$ K for Er_2CoGa_8, and $\mathcal{J}_{ex}^{ab}/k_B=-0.53$ K and $\mathcal{J}_{ex}^{c}/k_B=-0.075$ K for Tm_2CoGa_8.

In Er_2CoGa_8 $\mathcal{J}_{ex}^{c}$ is approximately equal to $\mathcal{J}_{ex}^{ab}$. Our results show that this scenario favors a (+−+−) AFM stacking of planes, with an equivalent, anisotropic AFM coupling in the *ab* plane, along the *b* axis. By comparison, in Tm_2CoGa_8 $\mathcal{J}_{ex}^{c}$ is small compared to the large $\mathcal{J}_{ex}^{ab}$ value. The magnetic structure is therefore dominated by a strong, in-plane AFM coupling with a favored (++−−) *c*-axis stacking. Our refined magnetic structures are consistent with, and reinforce, the calculated CEF-dependent exchange constants. Importantly, this shows that by choice of the rare-earth ion one can modify the CEF within the R_2CoGa_8 series in order to predetermine the magnetic structure.

The R_2CoGa_8 crystal structure can be thought of as a stacking of RGa_3 units, separated by $CoGa_2$ layers. By comparing RGa_3 to R_2CoGa_8, the similar *a* lattice parameter and the requirement of heavier rare-earth mass for stable crystallization suggests that the RGa_3 units are key building blocks in the formation of the ternary compound.[11] An analogous argument is also made for R_2CoIn_8 (Refs. 8 and 11) and Ce_2RhIn_8 (Ref. 26) compounds. Indeed, in Ce_2RhIn_8 this is supported by the common rare-earth magnetic structures of Ce_2RhIn_8 and $CeIn_3$.[26] This suggests that the $RhIn_2$ layers have little influence on the magnetic structure, giving 2D characteristics. We note that this is not the case in the R_2CoGa_8 series. The simple collinear magnetic structures refined in this paper do not reflect the more complicated magnetic structures of the RGa_3 (R = Er and Tm) compounds.[27] For example, the $TmGa_3$ magnetic structure is multiaxial, involving two or three propagation vectors. Indeed, the evaluation of the critical exponent predicts a magnetic structure that is three-dimensional. Further work is required to understand the role of the $CoGa_2$ layers and their counterparts in the other intermetallics, particularly when considering the dimensionality of the magnetic structure.

IV. CONCLUSIONS

We have solved the magnetic structure of two, newly synthesized intermetallic compounds, Er_2CoGa_8 and Tm_2CoGa_8. In both materials, magnetic moments were refined and found to lie parallel to the *b* axis, with magnitudes $4.71(3)\mu_B$/Er and $2.35(4)\mu_B$/Tm. Despite having common easy axes of magnetization (in the *ab* plane) the magnetic propagation vectors were found to be different; in Er_2CoGa_8 $\mathbf{k}=(0,1/2,0)$ and in Tm_2CoGa_8, $\mathbf{k}=(1/2,0,1/2)$. The different magnetic structures are due to a competition between crystal electric field effects and the RKKY exchange interaction. We show that the magnetic order parameter adopts either the 3D-Ising or 3D-XY universality class, with transition temperatures of 3.0 K and 2.0 K, for the erbium and thulium compounds, respectively. Further, by comparison of the R_2CoGa_8 and RGa_3 magnetic structures, we suggest that the $CoGa_2$ layers play an important role in the 3D magnetism in this series, as opposed to inducing a quasi-2D magnetic structure as in Ce_2RhIn_8.

ACKNOWLEDGMENTS

R.D.J. would like to thank Stewart Bland for helpful discussions. R.D.J., T.F., and P.D.H. would like to thank STFC (U.K.) and EPSRC (U.K.) for funding. C.A., C.G., and P.G.P. acknowledge support from FAPESP (SP-Brazil), CNPq (Brazil), and CAPES (Brazil).

*r.d.johnson@durham.ac.uk

[1] G. Chen, S. Ohara, M. Hedo, Y. Uwatoko, K. Saito, M. Sorai, and I. Sakamoto, J. Phys. Soc. Jpn. **71**, 2836 (2002).

[2] M. Nicklas, V. A. Sidorov, H. A. Borges, P. G. Pagliuso, C. Petrovic, Z. Fisk, J. L. Sarrao, and J. D. Thompson, Phys. Rev. B **67**, 020506(R) (2003).

[3] I. Sugitani *et al.*, J. Phys. Soc. Jpn. **75**, 043703 (2006).

[4] N. Kimura, Y. Muro, and H. Aoki, J. Phys. Soc. Jpn. **76**, 051010 (2007).

[5] E. Bauer, H. Kaldarar, A. Prokofiev, E. Royanian, A. Amato, J. Sereni, W. Bramer-Escamilla, and I. Bonalde, J. Phys. Soc. Jpn. **76**, 051009 (2007).

[6] P. G. Pagliuso *et al.*, J. Appl. Phys. **99**, 08P703 (2006).

[7] R. Settai, T. Takeuchi, and Y. Onuki, J. Phys. Soc. Jpn. **76**,

051003 (2007).
[8] D. A. Joshi, C. V. Tomy, and S. K. Malik, J. Phys.: Condens. Matter **19**, 136216 (2007).
[9] F. Steglich, J. Aarts, C. D. Bredl, W. Lieke, D. Meschede, W. Franz, and H. Schafer, Phys. Rev. Lett. **43**, 1892 (1979).
[10] A. Szytula and J. Leciejewicz, *Handbook of Crystal Structures and Magnetic Properties of Rare Earth Intermetallics* (CRC Press, Boca Raton, 1994).
[11] D. A. Joshi, R. Nagalakshmi, S. K. Dhar, and A. Thamizhavel, Phys. Rev. B **77**, 174420 (2008).
[12] D. A. Joshi, A. K. Nigam, S. K. Dhar, and A. Thamizhavel, Phys. Rev. B **80**, 054414 (2009).
[13] C. Adriano, L. Mendonca-Ferreira, E. M. Bittar, and P. G. Pagliuso, J. Appl. Phys. **103**, 07B712 (2008).
[14] D. Kaczorowski, A. P. Pikul, D. Gnida, and V. H. Tran, Phys. Rev. Lett. **103**, 027003 (2009).
[15] C. Adriano, C. Giles, L. N. Coelho, and P. G. Pagliuso, Physica B **404**, 3289 (2009).
[16] Z. Fisk and J. P. Remeika, *Handbook on the Physics and Chemistry of Rare Earths* (Elsevier, New York, 1989), Vol. 12.
[17] http://www.isis.rl.ac.uk/
[18] J. Rodríguez-Carvajal, Physica B **192**, 55 (1993).
[19] M. F. Collins, *Magnetic Critical Scattering* (Oxford University Press, Oxford, 1989).
[20] W. E. Wallace, *Rare Earth Intermetallics* (Academic Press, New York, 1973).
[21] S. C. Miller and W. F. Love, *Tables of Irreducible Representations of Space Groups and Co-Representations of Magnetic Space Groups* (Preutt Press, Boulder, 1967).
[22] http://www.mcphase.de
[23] D. B. Litvin, Acta Crystallogr., Sect. A: Found. Crystallogr. **64**, 419 (2008).
[24] C. D. Routsi, J. K. Yakinthos, and E. Gamari-Seale, J. Magn. Magn. Mater. **116**, 397 (1992).
[25] E. A. Goremychkin, R. Osborn, B. D. Rainford, R. T. Macaluso, D. T. Adroja, and M. Koza, Nat. Phys. **4**, 766 (2008).
[26] W. Bao, P. G. Pagliuso, J. L. Sarrao, J. D. Thompson, Z. Fisk, and J. W. Lynn, Phys. Rev. B **64**, 020401(R) (2001).
[27] P. Morin, M. Giraud, P. L. Regnault, E. Roudaut, and A. Czopnik, J. Magn. Magn. Mater. **66**, 345 (1987).